SCIENTIFIC REPORTS

OPEN

SUBJECT AREAS:
NANOPHOTONICS AND PLASMONICS
SUB-WAVELENGTH OPTICS
POLARITONS
APPLIED PHYSICS

Received
28 May 2013

Accepted
17 September 2013

Published
8 October 2013

Correspondence and requests for materials should be addressed to B.Z. (bez210@lehigh.edu) or F.J.B. (fjb205@lehigh.edu)

Ultrathin Nanostructured Metals for Highly Transmissive Plasmonic Subtractive Color Filters

Beibei Zeng, Yongkang Gao & Filbert J. Bartoli

Electrical and Computer Engineering Department, Lehigh University, Bethlehem, PA 18015.

Plasmonic color filters employing a single optically-thick nanostructured metal layer have recently generated considerable interest as an alternative to colorant-based color filtering technologies, due to their reliability, ease of fabrication, and high color tunability. However, their relatively low transmission efficiency (~30%) needs to be significantly improved for practical applications. The present work reports, for the first time, a novel plasmonic subtractive color filtering scheme that exploits the counter-intuitive phenomenon of extraordinary low transmission (ELT) through an ultrathin nanostructured metal film. This approach relies on a fundamentally different color filtering mechanism than that of existing plasmonic additive color filters, and achieves unusually high transmission efficiencies of 60 ~ 70% for simple architectures. Furthermore, owing to short-range interactions of surface plasmon polaritons at ELT resonances, our design offers high spatial resolution color filtering with compact pixel size close to the optical diffraction limit (~λ/2), creating solid applications ranging from imaging sensors to color displays.

Nanopatterned ultrathin metal films are investigated for use as highly transmissive plasmonic subtractive color filter arrays with sub-micrometer spatial resolution. This represents an attractive approach for on-chip color filters, which are vital components for future displays, image sensors, digital photography, projectors and other optical measurement instrumentation. Previous approaches based on traditional colorant filters employ organic dyes or chemical pigments that are vulnerable to processing chemicals, and undergo performance degradation under long-duration ultraviolet irradiation or at high temperatures. Furthermore, highly-accurate lithographic alignment techniques are required to pattern each type of pixel in a large-area array, significantly increasing fabrication complexity and cost. Plate-like dielectric deflectors have recently been proposed[1], but this scheme suffers from intrinsic limitations due to poor color purity, since the deflector covers only half of the total area. Nanoplasmonic color filters have been proposed recently as a promising means of overcoming the above limitations[2–11].

The well-known extraordinary optical transmission (EOT) phenomenon[12–14], observed in a single optically-thick metal film perforated with a periodic subwavelength hole array, has been extensively studied for additive color filtering (ACF) applications over the past decade. Such plasmonic color filters reject the entire visible spectrum except for selective transmission bands that are associated with the excitation of surface plasmon polaritons (SPPs)[2,6–14]. These EOT transmission bands can be spectrally tuned throughout the entire visible spectrum by simply adjusting geometric parameters, such as the periodicity, shape and size of nanoholes, leading to the high color tunability. Single-layer nanostructured metals also have significant advantages over colorant-based materials due to their ease of fabrication and device integration, and greater reliability under high temperature, humidity and long-term radiation exposure[2,7–9]. Despite these advantages, the low transmission efficiency of hole-array plasmonic ACFs (~30% at visible wavelengths) remains a bottleneck that limits their commercial applications[8]. Recently, peak transmission efficiencies of 40 ~ 50% were achieved in the state-of-art hole-array plasmonic ACFs[2], but at the expense of spectral bandwidth and color crosstalk. This transmission efficiency is still far below that of commercial image sensors (~80%, FUJIFILM Electronic materials U.S.A., Inc.). Plasmonic ACFs formed by metal-insulator-metal (MIM) or metal-dielectric (MD) waveguide nanoresonators have achieved high transmission efficiencies of 50 ~ 80%[3,10,11], but are not suitable for low-cost nanofabrication and device integration due to their complex multilayer designs. There is still a critical need for novel plasmonic color filters with both high transmission efficiency and simple cost-effective architectures.

The present work explores the counter-intuitive extraordinary low transmission (ELT) phenomenon in a single optically-thin (30 *nm*-thick) Ag film patterned with one dimensional (1D) nanogratings[15–21], and reports a novel

approach to achieving plasmonic subtractive color filters (SCFs) with unusually high transmission of 60 ~ 70%. In this subtractive color filtering scheme, specific colors (i.e. cyan, magenta, and yellow, CMY) are generated by removing their complementary components (i.e. red, green, and blue, RGB) from the visible spectrum. Due to their broad passbands with twice the photon throughput of narrow-band ACFs, SCFs have the major advantages of better light transmission and a stronger color signal, and have been successfully used in image sensors for years[22,23]. Unfortunately, highly efficient plasmonic SCFs have not previously been proposed or realized. The present work exploits recent advances in thin-film plasmonic nanostructures, and achieves for the first time, plasmonic SCFs with high transmission efficiency close to that for commercial image sensors. The transmission minima of plasmonic SCFs, corresponding to the ELT resonances, can be arbitrarily tuned to specific wavelengths across the entire visible region by simply varying the geometric parameters of nanogratings. Moreover, owing to short-range interactions of SPPs between nearest-neighbor nanostructures at the ELT resonances, plasmonic SCFs can efficiently filter colors with only a few (even only two) nanoslits, yielding ultracompact pixel sizes close to the optical diffraction limit (~λ/2, i.e. 200 ~ 350 *nm*) that determines the highest achievable optical resolution[4,24]. Therefore, plasmonic SCFs are capable of providing even smaller pixel sizes than those currently achieved in commercial image sensors (1.12 × 1.12 μm^2, Sony Corp.). In addition, plasmonic SCFs with ultrathin 1D nanogratings considered here can be easily generalized to two-dimensional (2D) nanostructures (i.e. nanoholes, nanosquares) to achieve polarization-independent operation. It should be noted, however, that the polarization-dependent color filtering function of 1D plasmonic SCFs, which can either filter transverse-magnetic (TM) polarized illumination or function as transparent windows under transverse-electric (TE) polarization, makes them highly attractive for next-generation transparent displays[25,26].

Results

Ultrathin plasmonic subtractive color filters based on extraordinary low transmission. Figure 1 (a) is a photograph of a 30 *nm*-thick Ag film deposited on a standard microscope glass slide. The background pattern can be clearly seen through the semi-transparent Ag film. The Ag film thickness is determined to be 29.8 *nm*. Its optical constants are noticeably different from those of an optically thick (350 *nm*) Ag film (Supplementary Figure S1). A schematic diagram of the proposed plasmonic SCFs is shown in Figure 1 (b), where 1D nanogratings with different periods are patterned on the ultrathin Ag film. For normally incident light polarized along the *x*-direction (TM polarization), the absorption and reflection are enhanced at the resonance wavelength[15–21], leading to a transmission minimum, which is opposite to the well-known EOT phenomenon that exhibits enhanced transmission peak at the resonance wavelength in optically-thick nanostructured metal films[12–14]. By simply varying the period of nanopatterns on the ultrathin metal film, arbitrary colors may be subtracted from broadband white light. The key features of this design, which contains only a single ultrathin nanopatterned metal layer, are their simple design rules, ease of fabrication, and scalable throughput by means of large-area nanofabrication methods, such as nanoimprint lithography or optical interference lithography[27–29]. For a proof-of-principle experiment, nanogratings with different periods were fabricated using focus ion beam (FIB) milling. The right column in Figure 1 (c) shows scanning electron microscopy (SEM) images of the fabricated nanogratings with three different periods (230 *nm*, 270 *nm* and 350 *nm*). The duty cycle of nanogratings was set as 0.5 for convenience. Figure 1 (c) presents measured transmission spectra of the cyan (P = 350 *nm*), magenta (P = 270 *nm*) and yellow (P = 230 *nm*) plasmonic SCFs under TM-polarization (Supplementary Figure S2), with transmission minima

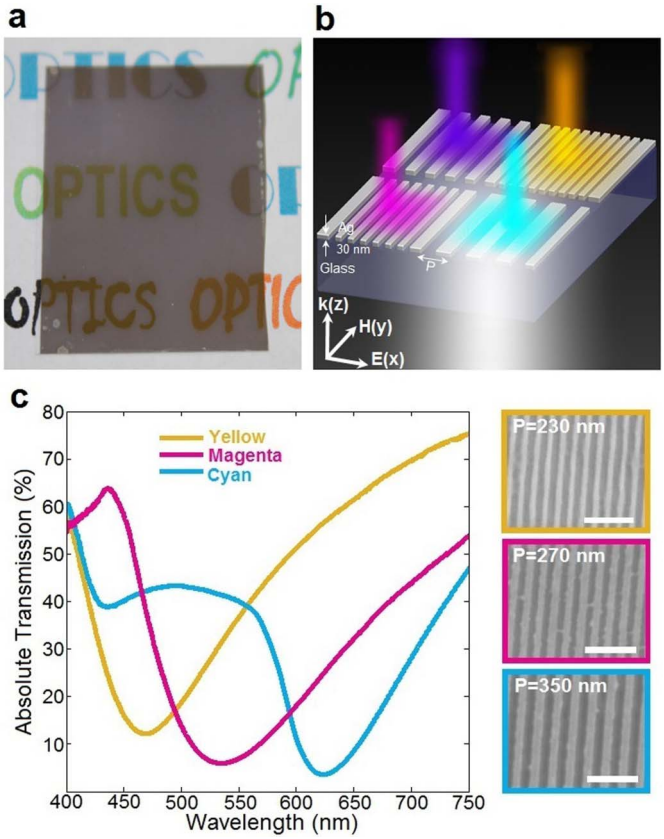

Figure 1 | Plasmonic subtractive color filters formed by ultrathin Ag nanogratings. (a) A photograph of a 30 *nm*-thick semi-transparent Ag film deposited on a microscope glass slide, showing the words "OPTICS" in the background. (b) Schematic diagram of the proposed plasmonic SCFs. White light is incident from the glass side, and the cyan, magenta, purple and yellow beams represent the transmitted colored light through 30 *nm*-thick Ag nanogratings with different periods. (c) Measured TM transmission spectra for yellow, magenta and cyan plasmonic SCFs consisting of 30 *nm*-thick Ag nanogratings with periods of 230 *nm*, 270 *nm* and 350 *nm*, respectively. Right column shows corresponding SEM images of the fabricated nanogratings. Scale bars are 1 μm.

that are positioned in red, green, and blue spectral regions, respectively. Note that the observed absolute peak transmission, 60 ~ 70% in the visible region, represent an unusually high transmission efficiency for such structures[2,3,6–14]. The full-widths at half maximum (FWHM) of the stopbands are approximately 100 *nm* for yellow and cyan SCFs, and 160 *nm* for magenta SCFs, which are comparable to the passband width for state-of-art plasmonic ACFs[2,3].

The solid cyan and black curves in Figure 2 represent the measured transmission spectra under TM-polarized illumination through 30 *nm*-thick Ag films with and without 340 *nm*-period nanogratings, respectively. The intriguing characteristic of ELT phenomenon is that the optical transmission through the ultrathin Ag film patterned with nanogratings (solid or dashed cyan curves) is lower than that through the unpatterned Ag film (10 ~ 12%, solid or dashed black curves) over a broad spectral range (gray region), even though 50% of the highly-reflective Ag is removed in the nanogratings compared to the unpatterned Ag film. The 6% experimental transmission minimum centered at a wavelength of 610 *nm* is consistent with the finite-difference time-domain (FDTD) simulations (dashed cyan curves). It should be noted that the calculated transmission minimum is close to zero (0.39%), indicating that the incident light can in principle be completely blocked by the ultrathin nanogratings

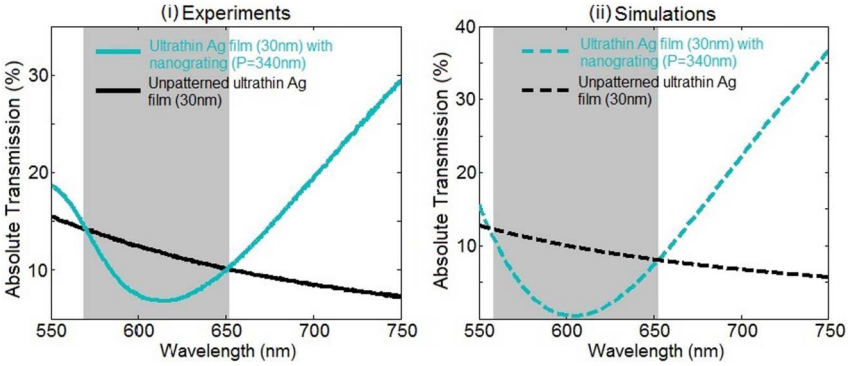

Figure 2 | Verification of Extraordinary low transmission in ultrathin Ag nanogratings. Measured (i) and simulated (ii) TM transmission spectra through 30 *nm*-thick Ag films with nanogratings of period P = 340 *nm* (cyan curves) compared to that for the unpatterned film (black curves). The ELT phenomenon occurs in the gray spectral region.

at the resonance wavelength. Differences between the experimental and numerical results can be attributed to the nonparallel incident light employed in the measurement, nanofabrication defects, surface roughness, and finite periodicity. The simulated transmission (T), reflection (R) and absorption (A) for this 30 *nm*-thick Ag nanograting with P = 340 *nm* are 0.39%, 85.5% and 14.11%, respectively, at the ELT resonance wavelength. Note that T = 10.9%, R = 82.86% and A = 6.24% for the case of the unpatterned film. The increased reflection and absorption result in the suppression of the transmission in ultrathin Ag nanogratings.

In order to achieve a full palette of subtractive colors that spans the entire visible region, the period of nanogratings was varied from 220 *nm* to 360 *nm* in 10 *nm* increments. All the fabricated nanogratings have the same dimensions of 10 × 10 μm^2. Figure 3 (a) shows the corresponding optical microscope images (from yellow to cyan) of fifteen square-shaped plasmonic SCFs illuminated by TM-polarized white light. At the same time, these nanostructures strongly transmit TE-polarized light (Supplementary Figure S3), which distinctly contrasts with that of previous optically-thick plasmonic ACFs or wire-grid polarizers[3,30]. The polarization-dependent color filtering effects in plasmonic SCFs arise from the polarization-dependent excitation of SPPs in 1D Ag nanogratings. This unique feature indicates that the proposed plasmonic SCFs can function either as SCFs or highly transparent windows under different polarizations, which has potential applications in transparent displays[25,26]. Figure 3 (b) presents transmission spectra of the plasmonic SCFs, exhibiting transmission minima that are tuned across the visible spectrum by varying the period from 220 *nm* to 360 *nm*. FDTD simulations (i) agree reasonably well with the experimental results (ii). The trend lines (dashed black lines) approximate the variation of transmission minima from 470 *nm* to 620 *nm* as the periods change from 220 *nm* to 360 *nm*. The variation of the transmission minima with period are further illustrated in Figure 3 (c), showing a nearly linear relation between the resonance wavelengths and nanograting period. That arbitrary subtractive colors can be obtained by simply varying the grating period is highly advantageous. This could extend

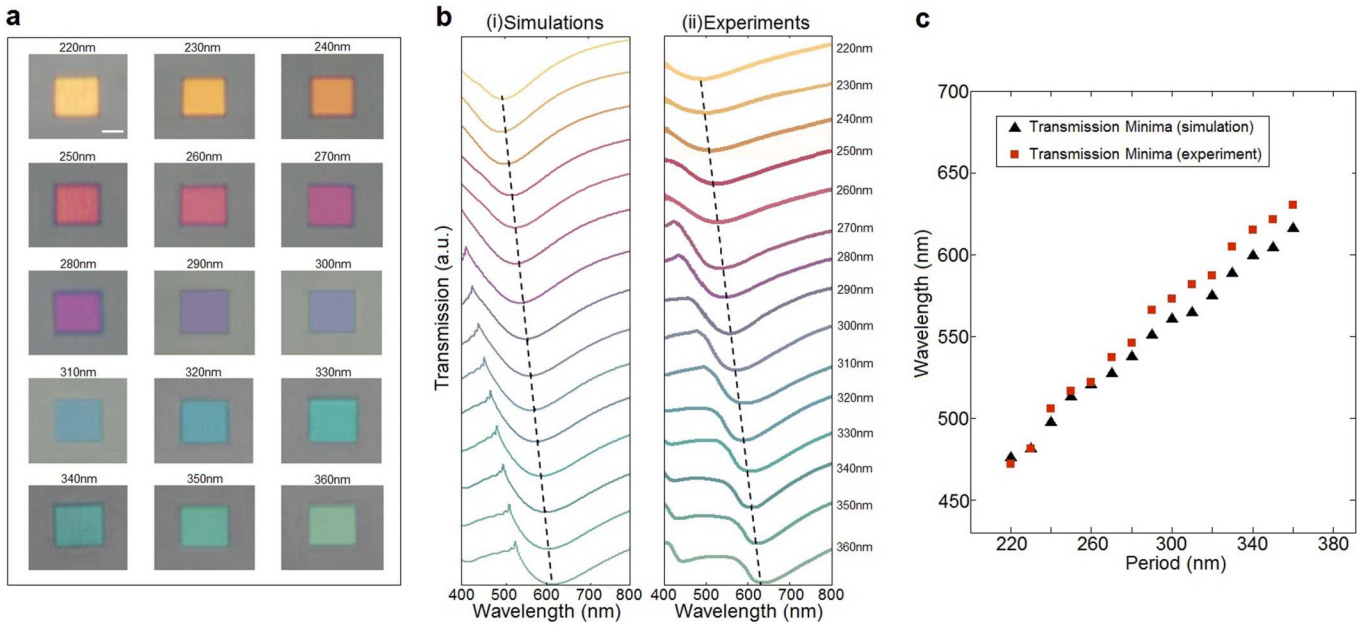

Figure 3 | Optical micrographs and spectral analyses of ultrathin plasmonic subtractive color filters with varying periods. (a) The full palette of transmitted subtractive colors from yellow to cyan is revealed in above 10 × 10 μm^2 squares under TM-polarized white light illumination, as the nanograting period changes from 220 *nm* to 360 *nm* in 10 *nm* increments. The scale bar is 5 μm. (b) Simulated (i) and experimental (ii) TM transmission spectra of nanogratings with periods ranging from 220 *nm* to 360 *nm*. The trend lines (dashed black lines) approximate the change of the transmission minima with varying grating period. (c) Correlation between transmission minima observed in the experimental (red square) and simulation (black triangle) data.

the operational range of conventional colorant color filters that do not scale well to more than three spectral bands, making them especially attractive for multispectral imaging applications[6].

Physical mechanisms responsible for extraordinary low transmission. The phenomenon of ELT in ultrathin nanopatterned metal film has been the subject of numerous fundamental investigations since 2009[15–21]. Although there is a general agreement that SPPs play a crucial role in ELT, recent studies have reported different conclusions regarding whether the suppression of transmission is due to the excitation of short-range SPPs (SRSPPs) or localized SPPs (LSPPs)[17,18]. To elucidate the physical mechanisms underlying the ELT phenomenon, we model the optical properties of ultrathin Ag nanogratings via FDTD simulations. 2D maps of the calculated transmission, absorption and reflection for 30 *nm*-thick Ag nanogratings are shown in Figure 4 (a)–(c), respectively, as a function of the incident wavelength and grating period. The duty cycle of nanogratings is set as 0.5. The low-transmission band in Figure 4 (a) shifts to longer wavelengths as the grating period increases.

The resonance wavelengths of the lowest and higher orders SRSPP modes were calculated using analytical dispersion relations (see Methods), and plotted in Figure 4 (a)–(c) as solid and dash-dotted white curves, respectively. The contribution of LSPP modes was estimated by calculating the spectral positions of LSPPs for single Ag lines (with the same line-width as that of nanogratings). These are represented by the dashed white line in Figure 4 (a)–(c). Both SRSPP and LSPP modes exhibit spectral dependence on the grating period (line-width) that is in reasonable agreement with the FDTD simulations. The simulated transmission minima and absorption/reflection peaks, which vary continuously from 400 *nm* to 650 *nm* in wavelength as the period increases from 100 *nm* to 400 *nm*, are located in between the dashed (LSPP) and solid white curves (SRSPP). This indicates that LSPP and SRSPP modes both contribute to the ELT

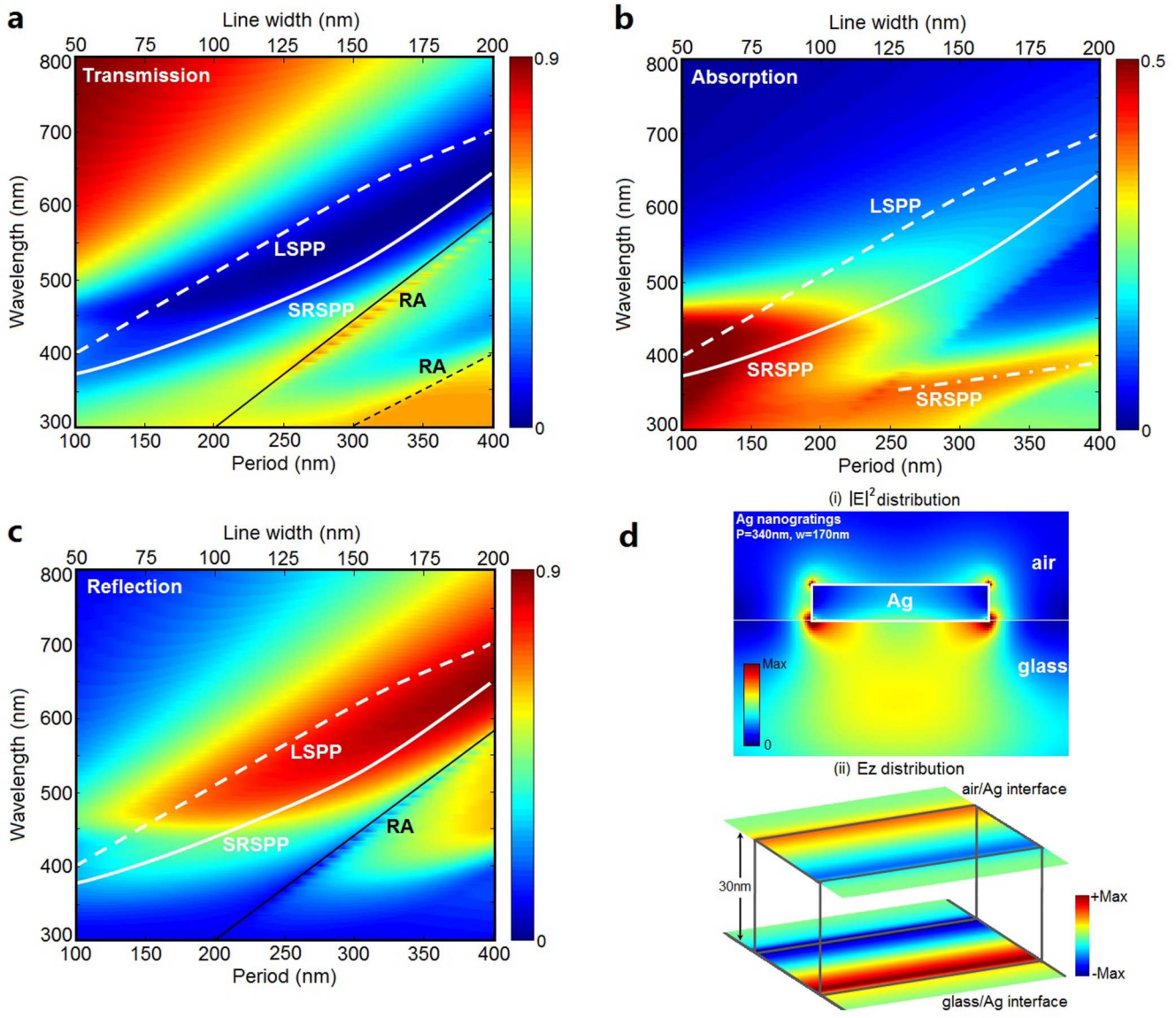

Figure 4 | Theoretical clarification of extraordinary low transmission in ultrathin Ag nanogratings. 2D maps of the calculated TM optical transmission (a), absorption (b) and reflection (c) spectra of 30 *nm*-thick Ag nanogratings as a function of the incident wavelength and grating period, when the duty cycle of the nanogratings is set at 0.5. The solid and dashed black lines refer to RA at glass/Ag and air/Ag interfaces, respectively. The solid and dash-dotted white curves correspond to the analytical dispersion relations for the lowest and higher orders SRSPP modes, respectively. The dashed white line represents the calculated spectral positions of LSPP for single Ag lines with the same line-width as that of nanogratings. (d) Electric field (i) and instantaneous E_z vector (ii) distribution at the air/Ag and glass/Ag interfaces of nanogratings (P = 340 *nm*) at the resonance wavelength of 610 *nm*.

effect for the range of geometric parameters considered here. A narrow transmission peak attributed to Rayleigh-Wood anomalies (RA) at the Ag/glass interface (solid black line) ranges at shorter wavelengths[31,32]. The dashed black line in Figure 4 (a) represents the RA at the air/Ag interface, which matches well with a transmission peak in the ultraviolet region (300 ~ 400 *nm*). Figure 4 (a)–(c) show that for the range of geometric parameters considered in Figure 3, the transmission minima are primarily attributed to enhanced absorption and reflection in the Ag nanograting (Supplementary Figure S4), due to the excitation of SRSPP and LSPP modes.

To further characterize the electromagnetic modes at the resonance wavelength, we calculate the electric field (i) and E_z vector (ii) distributions at the air/Ag and glass/Ag interfaces for ultrathin nanogratings (P = 340 *nm*) at a wavelength of 610 *nm*. The results are plotted in Figure 4 (d), showing the excitation of propagating SPP modes[13]. The enhanced electromagnetic field (i) is strongly confined at the Ag/glass interface, with a decay length of hundreds of nanometers into the glass substrate. In addition, the antisymmetric E_z patterns (ii) correspond to a symmetric surface charge distribution (Supplementary Figure S5), further demonstrating the propagating SPP modes with the characteristics of SRSPPs[21]. Additional simulations reveal that the electromagnetic modes in a relatively broad spectral region close to the transmission minimum have similar E_z patterns. The electric field distribution (i) also shows LSPP modes (with a decay length of tens of nanometers) at the corners of nanogratings. Accordingly, the resonant electromagnetic modes in the ultrathin Ag nanogratings (duty cycle 0.5) have the properties of hybrid LSPP and SRSPP modes.

The FDTD simulations performed above, systematically varying geometric parameters such as periodicity and line-width (duty cycle 0.5), help to clarify the underlying physical mechanisms for ELT in ultrathin Ag nanogratings, and illustrate the relative contributions of the different electromagnetic modes (SRSPPs, LSPPs, and RA). For the range of geometric parameters used in our experiments (periods ranging from 220 to 360 *nm*), ELT results from the excitation of both SRSPP and LSPP modes that lead to enhanced absorption and reflection.

High-resolution plasmonic subtractive color filtering and applications. We now examine the functional relationship between plasmonic subtractive color filtering and feature size, to explore the achievable SCF spatial resolution and determine the smallest pixel size for imaging applications. Figure 5 (a) shows cyan and magenta plasmonic SCF arrays consisting of 2, 4, 6, 8 and 10 nanoslits, all with the same length of 15 μm and a duty cycle of 0.5. The nanoslit periods for the cyan and magenta SCFs are 350 *nm* and 270 *nm*, respectively. Surprisingly, the SCF arrays with only two nanoslits still exhibit distinct cyan (ii) or magenta (iii) colors. The nanoscale dimensions for the cyan and magenta filters with two nanoslits (525 *nm* and 405 *nm*, respectively) are close to the diffraction limit of visible light ($\lambda/2$, 200 ~ 350 *nm*)[4,24]. The electric field distributions were calculated for the cyan and magenta double-slit structures (Supplementary Figure S6). These simulations indicate that both SRSPP and LSPP modes are excited in these nanoscale doublet structures and contribute to the observed colors. Because of the short propagation distance of SRSPPs and small decay length of LSPPs, interactions between neighboring nanostructures are weaker than those for EOT phenomenon, where SPPs excited at each nanoslit (or nanohole) strongly interact with numerous nearby nanoslits (or nanoholes)[12–14]. Fewer repeat units are required in the proposed plasmonics SCFs than are commonly employed in plasmonic ACFs based on EOT theory. Additionally, Figure 5 (b) shows a series of cyan and magenta SCF structures fabricated with 2, 4, 6, 8 and 10 nanoslits, with slit lengths of 2, 1, 0.5, and 0.3 μm. The microscope images show that color filtering persists in the plasmonic SCFs with a few nanoslits even when the length of nanoslits is decreased to 0.3 μm (SEM images are shown in Supplementary Figure S7). Therefore, plasmonic SCFs are capable of generating much smaller pixel sizes (~0.5 × 0.3 μm^2) than the smallest pixels achieved today in commercial image sensors (1.12 × 1.12 μm^2, Sony Corp.). A unique feature of the plasmonic SCFs is their ability to perform color filtering on the nanometer scale, with much simpler and thinner structures than that of previous multilayered designs[3].

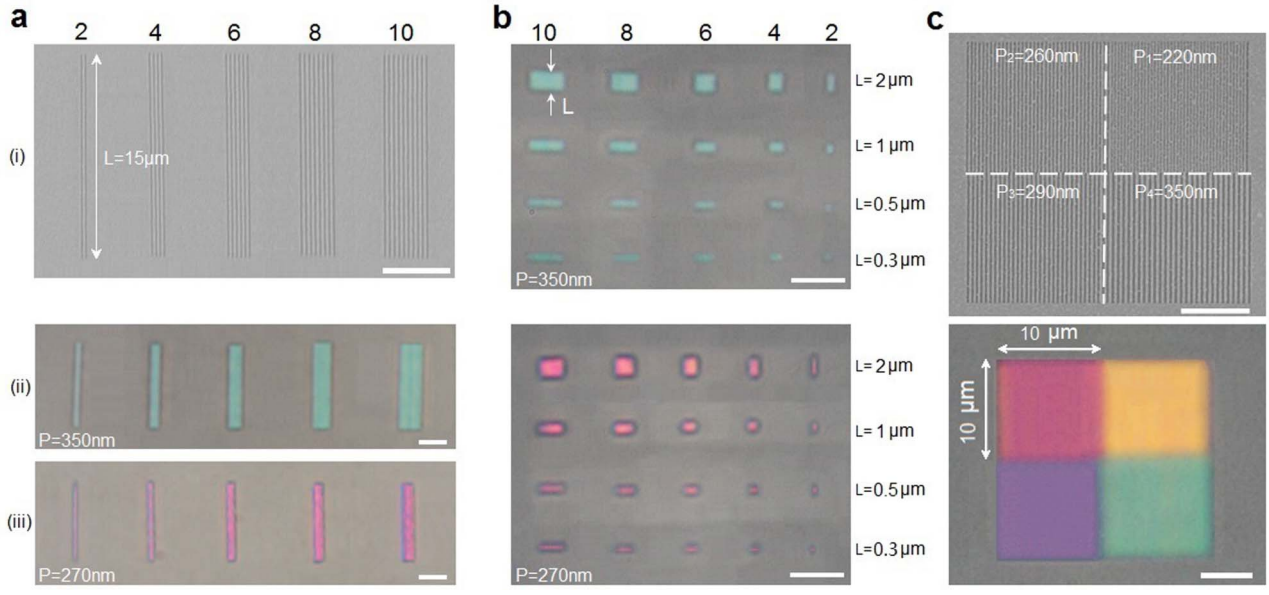

Figure 5 | Ultra-compact and high-resolution plasmonic subtractive color filters. (a) SEM image (i) of plasmonic SCFs with 2, 4, 6, 8 and 10 nanoslits of period P = 350 *nm*. (ii) and (iii) show the optical microscope images under TM illumination for the case of 2, 4, 6, 8 and 10 nanoslits with periods of 350 *nm* and 270 *nm*, respectively. (b) Optical microscope images of cyan (top panel, P = 350 *nm*) and magenta (bottom panel, P = 270 *nm*) plasmonic SCFs with 2, 4, 6, 8 and 10 nanoslits of differing lengths, ranging from 2 μm to 0.3 μm. (c) Top panel shows a SEM image of a plasmonic SCF mosaic consisting of four different 10 × 10 μm^2 color filter squares (nanogratings with different periods of P_1 = 220 *nm*, P_2 = 260 *nm*, P_3 = 290 *nm*, and P_4 = 350 *nm*) with zero separation. Bottom panel is the corresponding optical microscope image. All of the scale bars are 5 μm.

Additionally, Figure 5 (c) shows a 2 × 2 array of plasmonic SCFs fabricated to examine the effect of spatial crosstalk between adjacent structures on transmitted colors. This color filter mosaic consists of four different square-shaped (10 × 10 μm^2) plasmonic SCFs fabricated by FIB with zero separation. The four SCFs are composed of nanogratings with different periods (P_1 = 220 *nm*, P_2 = 260 *nm*, P_3 = 290 *nm*, and P_4 = 350 *nm*), as shown by the SEM images in the top panel of Figure 5 (c). The optical microscope image of the color filter mosaic under TM-polarized white light is shown in the bottom panel of Figure 5 (c). Four distinct subtractive colors can be clearly resolved even at the center corner or boundaries of adjacent filters, indicating that the proposed plasmonic SCFs can be applied to high-resolution color filter arrays widely used in imaging sensors or color displays[22,23,33]. The image blurring at boundaries arises from effects of light diffraction and the limited optical resolution of the microscope.

Spectral imaging combines two normally distinct techniques: imaging, in which the light intensity is typically measured at each pixel in a two dimensional array, and spectroscopic measurements of intensity as a function of wavelength, thus generating a three-dimensional multispectral data set I(x,y,λ). Applications of spectral imaging range from biological studies to remote sensing. However, this technique typically employs bulky filters and scanning interferometers to acquire a complete spectrum at each pixel[34], since conventional miniature color filter arrays are normally limited to three spectral bands (i.e. RGB or CMY)[3,6]. Recent studies of plasmonic miniature color filter arrays with wide color tunability were conducted to enable direct recording of spectral image data in a single exposure without scanning. These included plasmonic photon sorters (which had a limited transmission efficiency of 1.5 ~ 15%[6]) and an ultra-compact plasmonic spectroscope (composed of complex MIM nano-resonators[3]). In the current work, we employ plasmonic SCFs array to achieve a compact plasmonic subtractive spectroscope. Figure 6 (a) shows a SEM image of the fabricated device consisting of ultrathin nanogratings with periods gradually changing from 220 *nm* to 360 *nm* in increments of 1 *nm* and a fixed nanoslit width of 110 *nm*. When illuminated with TM-polarized white light, the structure produces a rainbow stripe of continuous subtractive colors, as shown in Figure 6 (b). This miniature plasmonic subtractive spectroscope can disperse the entire visible spectrum into component colors within a distance of a few micrometers, which is orders of magnitude smaller than the conventional prism- or grating-based devices for multispectral imaging[34]. This plasmonic subtractive spectroscope has a much higher transmission efficiency (60 ~ 70%), a simple scheme consisting of a single ultrathin nanopatterned metal film, which is five to ten times thinner than that of previous designs[3,6].

Next, we demonstrate the potential of plasmonic SCFs for transparent displays[25,26]. Figure 6 (c,i) shows an optical microscope image of a magenta character 'L' in a cyan background, formed when nanopatterns are illuminated with TM-polarized white light. The letter 'L' is constructed by nanogratings with a period of P = 270 *nm*, and the cyan background by nanogratings with a period of P = 350 *nm* (SEM images in Supplementary Figure S8). Two distinct colors are clearly preserved even at the sharp corners and boundaries between the two different patterns, indicating the high-resolution color filtering capability. Under TE polarized illumination, on the other hand, the same structure remains a transparent window, through which we can clearly observe a background object with its detailed features, as shown in Figure 6 (c,ii). This is quite different from that of the plasmonic nanoresonator ACFs, for which the TE-polarized incident light is totally blocked[3]. Therefore, the ultrathin plasmonic SCFs can function as color filters as an alternative to conventional colorant color filters and plasmonic ACFs, or act as a highly transparent window under illumination with a different polarization, offering a new approach for high-definition transparent displays through actively controlling the polarization of incident light at each color pixel.

Discussion

The theoretical simulations predict that ELT-based subtractive color filtering in ultrathin Ag nanogratings can achieve strong extinction within the resonance band, as well as high transmission peaks away from the resonance wavelength (i.e., 60 ~ 70% for a duty cycle of 0.5). This peak transmission is significantly larger than that (7 ~ 27%) of a closed Ag film of the same thickness. Moreover, since these structures are not optimized, further improvement may be possible, potentially achieving transmission values comparable to or even larger than that of commerical color filters. For example, we consider how the optical properties of plasmonic SCFs are affected by varying the grating duty cycle. The transmission away from the ELT resonance increases with the removal of highly-reflective Ag. Consequently, increasing the separation between neighboring Ag lines (i.e. varying the grating period while keeping the linewidth

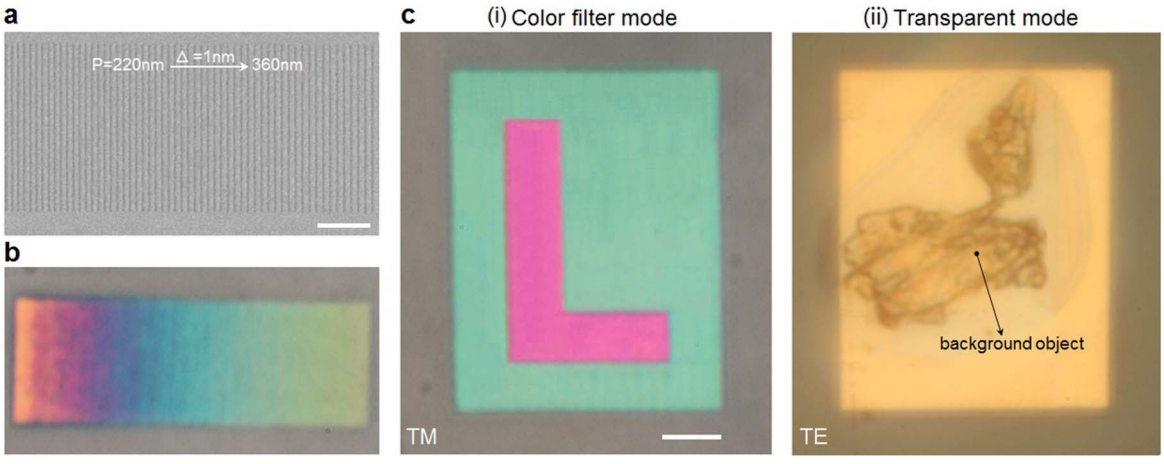

Figure 6 | Ultrathin plasmonic subtractive color filters for spectral imaging and transparent displaying. (a) A SEM image of the fabricated plasmonic subtractive spectroscope with grating periods gradually changing from 220 *nm* to 360 *nm* (from left to right, with 1 *nm* increment). The line-width of each nanoslit is fixed at 110 *nm*, and the scale bar represents 5 μm. (b) Optical microscope image of the plasmonic spectroscope illuminated with TM-polarized white light. (c) Optical microscope image of (i) a magenta pattern 'L' in a cyan background formed by nanogratings with two different periods (P_1 = 270 *nm*, P_2 = 350 *nm*) fabricated on a 30 *nm*-thick Ag film, and illuminated with TM-polarized white light. The scale bar is 10 μm. (ii) Imaging the background object through the same structure, under TE illumination.

fixed) would further enhance the transmission efficiency. However, the near-field coupling between adjacent Ag lines may also become less efficient as the separation is increased, potentially reducing the effectiveness of SRSPP modes relative to LSPP modes and affecting the ELT minimum. Therefore, the nanograting parameters (such as line-width, separation between adjacent lines, and period) should be varied judiciously to achieve simultaneous optimization of the SCF transmission efficiency and the on-resonance extinction.

Since the excitation of propagating SRSPP modes relies on the effective coupling of electromagnetic modes between Ag lines, we performed FDTD simulations to study the optical properties of ultrathin Ag nanogratings with a constant line-width as a function of the separation between adjacent Ag lines. Figure 7 (a) and (b) show 2D contour maps of the simulated transmission and absorption spectra for 30 *nm*-thick Ag nanogratings as a function of the incident wavelength and grating period, keeping the line-width of Ag wires fixed at 110 *nm*. For periods less than 150 *nm*, the broad transmission minimum in Figure 7 (a) in the 400 $nm < \lambda < 800$ *nm* spectral region is primarily due to high optical reflection, since the separation between adjacent Ag lines ($0 \sim 40$ nm) is very small. For nanogratings with $P > 150$ *nm*, excitation of SRSPPs and LSPPs in ultrathin Ag nanogratings causes enhanced absorption and reflection that affect the transmission minimum. The spectral transmission minimum narrows and appears less dependent on P with increasing period, suggesting less effective excitation of SRSPPs as the separation between adjacent Ag lines increases.

Figure 7 (b) illustrates the contributions of three different mechanisms to absorption enhancement. For periods in the range 150 $nm < P < 250$ *nm*, the separation between adjacent Ag lines ranges from 40 to 140 *nm*, and the absorption is mainly attributed to the excitation of SRSPP modes, as indicated by the analytical SRSPP dispersion curves (solid white curve). As the period increases further, the absorption spectra are closer to those predicted for LSPP modes (dashed white line). For periods greater than 300 *nm*, the electromagnetic modes excited in individual Ag lines do not couple effectively with each other due to the large separation (>190 *nm*) between adjacent lines. Finally, for $P > 350$ *nm*, RA modes (solid black curve) interact with SPPs, leading to a red-shift in absorption spectra.

The physical mechanisms are further illustrated by the calculated electric field distribution at the resonance wavelengths in these 30 *nm*-thick Ag nanogratings with a fixed 110 *nm* line-width. Grating periods of (i) 150 *nm*, (ii) 220 *nm*, and (iii) 380 *nm*, as well as (iv) a single Ag line were considered, and the results shown in Figure 7 (c). For the 150 *nm* period (i), with a 40 *nm* separation between grating lines, the electromagnetic modes excited in neighboring Ag lines strongly interact with each other. Both LSPP and SRSPP modes at the Ag/glass interface are clearly observed. For $P = 220$ *nm* (ii), the electromagnetic coupling between adjacent Ag lines is weaker than that in (i), but the excitation of SRSPP modes is still observable. For the 380 *nm* period (iii), the SRSPP modes are much less evident due to the large separation (270 *nm*) between adjacent Ag lines, and the field distribution approaches that of a single Ag line in (iv), which shows primarily LSPP modes. Slight differences in the resonance wavelengths between (iii) and (iv) arise due to the RA at the glass/Ag interface.

Although we have only demonstrated polarization-dependent plasmonic subtractive color filtering with 1D ultrathin nanogratings in this work, it can be easily generalized to 2D ultrathin nanostructures (i.e. nanoholes or nanosquares) for achieving polarization-independent operation. Nevertheless, the 1D plasmonic SCFs, which

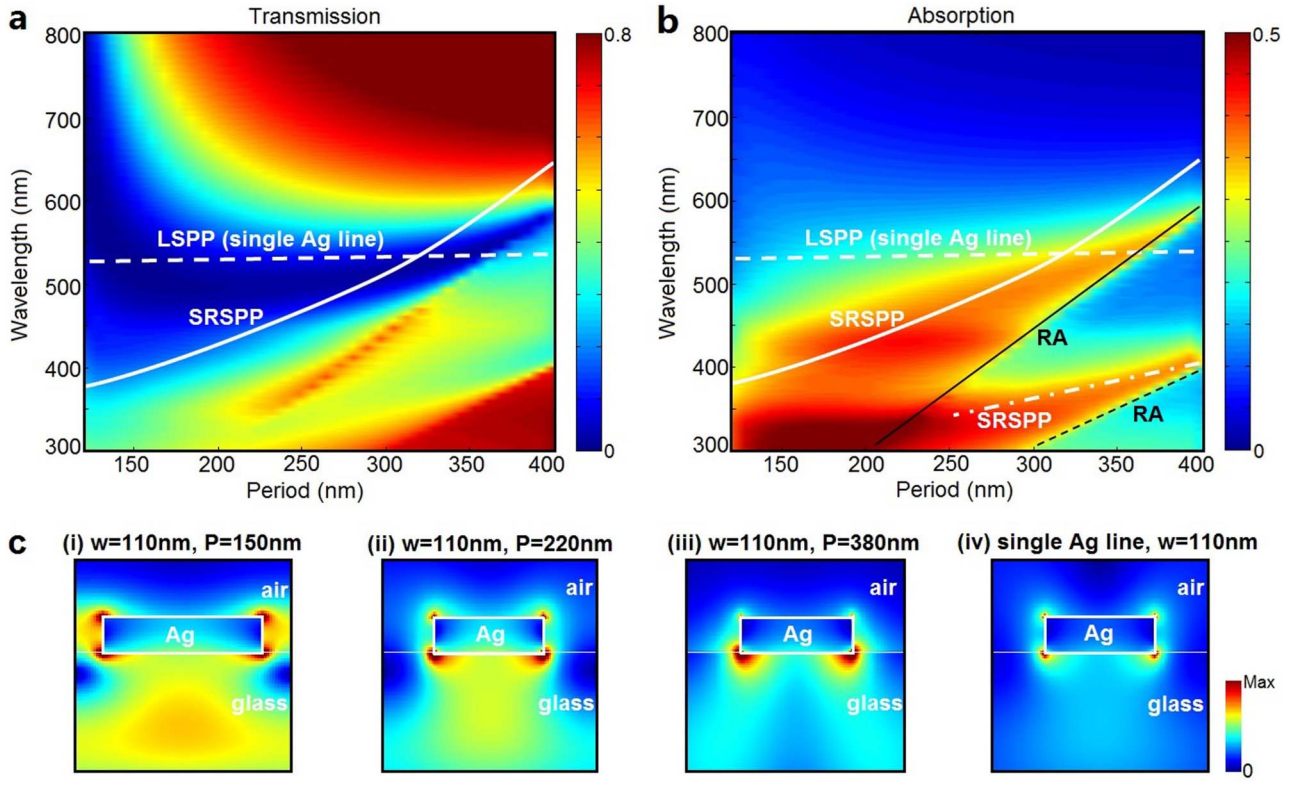

Figure 7 | Clarification of different electromagnetic modes in ultrathin Ag nanogratings. 2D maps of the calculated TM optical transmission (a) and absorption (b) spectra of 30 *nm*-thick Ag nanogratings as a function of the incident wavelength and grating period, when the line-width of individual Ag lines is fixed at 110 *nm*. The solid and dash-dotted white curves correspond to the analytical dispersion relations for the lowest and higher order SRSPP modes, respectively. And the dashed white line represents the spectral position of LSPP for a single Ag line with 110 *nm* line-width. The solid and dashed black lines in (b) refer to RA at glass/Ag and air/Ag interfaces, respectively. (c) Electric field distribution at the cross-section of ultrathin Ag nanogratings with the fixed line-width w = 110 *nm* and period of (i) 150 *nm*, (ii) 220 *nm*, (iii) 380 *nm*, and (iv) a single Ag line with the line-width of 110 *nm*.

can function either as color filters or highly transparent windows under different polarizations, making them highly attractive for transparent displaying[25,26]. In traditional transparent displays, the RGB color pixels of the color filter are reduced to the minimum size for transparency. Display panel makers even remove the color filter, making the transparent display monochrome. Therefore, the low resolution and color gamut are fundamental limitations in current transparent displaying techniques. The 1D plasmonic SCFs, which are capable of generating extremely small pixel sizes ($\sim 0.5 \times 0.3\ \mu m^2$) for high spatial resolution, could significantly advance this application area.

Discrepancies between the experimental and numerical results can be attributed to the nonparallel incident light employed in the optical measurement, nanofabrication defects, finite periodicity in the fabricated structures, and surface roughness, which are not considered completely in numerical simulations. Although the experimental transmission minimum (6%) differs appreciably with the numerical value of 0.39% in Figure 2, significant improvements should still be possible. The surface roughness (large grain size) in ultrathin Ag films is one of the factors that could significantly degrade the performance of plasmonic SCFs, possibly leading to measurement errors and non-uniform colors. Improved plasmonic SCF structures can be realized, for example, by introducing an intermediate (1 *nm*) Ge wetting layer before depositing Ag on the glass substrate or using template-stripping techniques[35–38], permitting ultra-smooth Ag films with smaller grain sizes for improved color filtering performance.

In summary, systematic theoretical and experimental studies were performed to clarify the underlying physical mechanisms that determine the ELT phenomenon. Different electromagnetic modes (SRSPPs, LSPPs, and RA) can be excited in ultrathin Ag nanogratings, depending on their geometric parameters. By exploiting ELT theory, we have proposed and demonstrated plasmonic SCFs associated with fundamentally different color filtering mechanisms than previous state-of-art plasmonic ACFs. The simple design, with its wide color tunability, ease of fabrication and device integration, as well as robustness and reliability, combines advances of SCFs and ultrathin plasmonic nanostructures to overcome key challenges in current colorant and plasmonic color filters. An unusually high transmission efficiency of 60 $\sim$ 70% has been achieved, with the potential for further enhancement. In addition, the proposed plasmonic SCFs are capable of generating even smaller pixel sizes than the smallest pixels achieved today in commercial image sensors. Finally, their unique polarization-dependent features allow the same structures to function either as color filters or highly-transparent windows under different polarizations, opening an avenue towards high-definition transparent displays. While only 1D nanograting structures have been demonstrated here, this design principle can be extended to 2D structures to achieve polarization-independent operation. The design can also be easily applied to other spectrum regimes for different applications.

Methods

Analytical SRSPP dispersion relations for ultrathin Ag films patterned with periodic subwavelength structures. For TM-polarized incident light, the two single-interface SPP modes at the top and bottom interfaces of ultrathin (30 *nm*) Ag nanogratings interact with each other, leading to coupled SPP modes, the long-range and short-range SPP (LRSPP and SRSPP) modes. The dispersion relations for LRSPP and SRSPP modes are described by the equation[18]:

$$\tanh(k_2 t)(\varepsilon_{d1}\varepsilon_{d2}k_2^2+\varepsilon_m^2 k_1 k_3)+\varepsilon_m k_2(\varepsilon_{d1}k_3+\varepsilon_{d2}k_1)=0 \quad (1)$$

Here $k_1^2=k_{spp}^2-\varepsilon_{d1}k_0^2$, $k_2^2=k_{spp}^2-\varepsilon_m k_0^2$, $k_3^2=k_{spp}^2-\varepsilon_{d2}k_0^2$, $k_0=\omega/c$ and t is the thickness of the metal film. ε_{d1} and ε_{d2} are dielectric constants of air and glass, and ε_m represent the dielectric constant of ultrathin (30 *nm*) Ag film. For the ultrathin Ag film with an asymmetric geometry ($\varepsilon_{d1} < \varepsilon_{d2}$), Eq. (1) yields strongly damped SRSPP modes with antisymmetric E_z field patterns at the air/Ag and glass/Ag interfaces. The momentum mismatch between SPP modes and free space light can be bridged by the reciprocal vectors of the periodic nanostructures $k_G = mG$, where $G = 2\pi/P$, P is the period, and m is an integer:

$$k_{spp}=k_0\sin\theta+mG \quad (2)$$

Here θ is the incident angle. For normal incidence ($\theta = 0^\circ$), the dispersion relations of the SRSPP modes are obtained by substituting Eq. (2) into Eq. (1). The solid and dash-dotted white curves in Figure 4 represent the analytical dispersion relations for the lowest and higher orders SRSPP modes, respectively.

Device fabrication and optical measurements. Ag films of 30 *nm* thickness were deposited by e-beam evaporation (Indel system) onto standard microscope slides (Fisherbrand), with a deposition rate of 0.1 nms^{-1}. Prior to the evaporation, the glass slides were cleaned thoroughly with acetone in an ultrasonic cleaner for 20 min, followed by extensive DI water rinsing. Focused ion beam (FEI Dual-Beam system 235) milling (30 kV, 30 pA) was used to fabricate the nanogratings on the ultrathin Ag films.

The optical properties of the nanofabricated structures were measured using an Olympus IX81 inverted microscope (The experimental apparatus employed for the measurement of transmission spectra is illustrated in Supplementary Figure S2). A 100 W halogen lamp was used as the white light source. The transmitted light was collected by a 40 $\times$ microscope objective with a numerical aperture of 0.6. The microscope field diaphragm and aperture stop were both closed in order to provide approximately collimated incident light. The collected light was coupled into a multimode fiber bundle interfaced with a compact spectrometer (Ocean Optics USB 4000). All optical images were obtained using a digital camera (Cannon EOS Rebel T3i).

Numerical simulations. Simulations of the transmission, reflection and absorption spectra were carried out by three-dimensional FDTD methods using the Lumerical commercial software package (Lumerical Solutions Inc.). The wavelength dependence of the optical constants of the ultrathin (30 *nm*-thick) Ag film was measured using a spectroscopic ellipsometer (J. A. Woolam), and incorporated into FDTD simulations. A unit cell consisting of one Ag strip was used with periodic boundary conditions to simulate an infinite array of periodic nanogratings. Perfectly matched layer boundary conditions were used in the vertical direction to prevent unphysical scattering at the edge of the simulation box. A uniform grid size of 2 *nm* was used in the calculation. To ensure convergence, the simulations were performed for differing grid sizes of 10 *nm*, 8 *nm*, 6 *nm*, 4 *nm* and 2 *nm*, and the results (transmission and reflection) clearly converged as the grid size varied from 6 nm to 2 *nm*.

1. Nishiwaki, S., Nakamura, T., Hiramoto, M., Fujii, T. & Suzuki, M. Efficient colour splitters for high-pixel-density image sensors. *Nat. Photonics* **7**, 240–246 (2013).
2. Yokogawa, S., Burgos, S. P. & Atwater, H. A. Plasmonic color filters for CMOS image sensor applications. *Nano Lett.* **12**, 4349–4354 (2012).
3. Xu, T., Wu, Y.-K., Luo, X. & Guo, L. J. Plasmonic nanoresonators for high resolution colour filtering and spectral imaging. *Nat. Commun.* **1**, 59 (2010).
4. Wu, Y.-K., Hollowell, A. E., Zhang, C. & Guo, L. J. Angle-Insensitive Structural Colours based on Metallic Nanocavities and Coloured Pixels beyond the Diffraction Limit. *Sci. Rep.* **3**, 1194 (2013).
5. Diest, K., Dionne, J. A., Spain, M. & Atwater, H. A. Tunable color filters based on metal–insulator–metal resonators. *Nano Lett.* **9**, 2579–2583 (2009).
6. Laux, E., Genet, C., Skauli, T. & Ebbesen, T. W. Plasmonic photon sorters for spectral and polarimetric imaging. *Nat. Photonics* **2**, 161–164 (2008).
7. Lee, H. S., Yoon, Y. T., Lee, S. S., Kim, S. H. & Lee, K. D. Color filter based on a subwavelength patterned metal grating. *Opt. Express* **15**, 15457–15463 (2007).
8. Chen, Q. & Cumming, D. R. High transmission and low color cross-talk plasmonic color filters using triangular-lattice hole arrays in aluminum films. *Opt. Express* **18**, 14056–14062 (2010).
9. Inoue, D. *et al.* Polarization independent visible color filter comprising an aluminum film with surface-plasmon enhanced transmission through a subwavelength array of holes. *Appl. Phys. Lett.* **98**, 093113 (2011).
10. Kaplan, A. F., Xu, T. & Guo, L. J. High efficiency resonance-based spectrum filters with tunable transmission bandwidth fabricated using nanoimprint lithography. *Appl. Phys. Lett.* **99**, 143111 (2011).
11. Yoon, Y. T., Park, C. H. & Lee, S. S. Highly efficient color filter incorporating a thin metal-dielectric resonant structure. *Appl. Phys. Express* **5**, 022501 (2012).
12. Ebbesen, T. W., Lezec, H. J., Ghaemi, H. F., Thio, T. & Wolff, P. A. Extraordinary optical transmission through subwavelength hole arrays. *Nature* **391**, 667–669 (1998).
13. Barnes, W. L., Dereux, A. & Ebbesen, T. W. Surface plasmon subwavelength optics. *Nature* **424**, 824–830 (2003).
14. Genet, C. & Ebbesen, T. W. Light in tiny holes. *Nature* **445**, 39–46 (2007).
15. Spevak, I. S., Nikitin, A. Y., Bezuglyi, E. V., Levchenko, A. & Kats, A. V. Resonantly suppressed transmission and anomalously enhanced light absorption in periodically modulated ultrathin metal films. *Phys. Rev. B* **79**, 161406 (2009).
16. Rodrigo, S. G. *et al.* Extraordinary optical transmission through hole arrays in optically thin metal films. *Optics Lett.* **34**, 4–6 (2009).
17. D'Aguanno, G., Mattiucci, N., Alu, A. & Bloemer, M. J. Quenched optical transmission in ultrathin subwavelength plasmonic gratings. *Phys. Rev. B* **83**, 035426 (2011).

18. Braun, J., Gompf, B., Kobiela, G. & Dressel, M. How holes can obscure the view: suppressed transmission through an ultrathin metal film by a subwavelength hole array. *Phys. Rev. Lett.* **103**, 203901 (2009).
19. Xiao, S. *et al.* Nearly zero transmission through periodically modulated ultrathin metal films. *Appl. Phys. Lett.* **97**, 071116 (2010).
20. Xiao, S. & Mortensen, N. A. Surface-plasmon-polariton-induced suppressed transmission through ultrathin metal disk arrays. *Opt. Lett.* **36**, 37–39 (2011).
21. Gan, Q. *et al.* Short Range Surface Plasmon Polaritons for Extraordinary Low Transmission Through Ultra-Thin Metal Films with Nanopatterns. *Plasmonics* **7**, 47–52 (2012).
22. Nabeyama, H., Nagahara, S., Shimizu, H., Noda, M. & Masuda, M. All solid state color camera with single-chip MOS imager. *IEEE Trans. Consumer Electron.* **CE-27**, 40–46 (1981).
23. Sencar, H. T. & Memon, N. *Digital Image Forensics: Advances and Challenges.* (Springer, New York, 2012).
24. Kumar, K. *et al.* Printing colour at the optical diffraction limit. *Nat. Nanotech.* **7**, 557–561 (2012).
25. Seo, H.-S. Transparent display apparatus. U.S. Patent No. 8227797 (2012).
26. Azuma, R. *et al.* Recent Advances in Augmented Reality. *IEEE Comput. Graph. Appli.* **21**, 34–47 (2001).
27. Chou, S. Y., Krauss, P. R. & Renstrom, P. J. Imprint lithography with 25-nanometer resolution. *Science* **272**, 85–87 (1996).
28. Luo, X. & Ishihara, T. Surface plasmon resonant interference nanolithography technique. *Appl. Phys. Lett.* **84**, 4780–4782 (2004).
29. Zeng, B., Yang, X., Wang, C. & Luo, X. Plasmonic interference nanolithography with a double-layer planar silver lens structure. *Opt. Express* **17**, 16783–16791 (2009).
30. Wang, J. *et al.* High-performance nanowire-grid polarizers. *Opt. Lett.* **30**, 195–197 (2005).
31. Wood, R. W. On a remarkable case of uneven distribution of light in a diffraction grating spectrum. *Philos. Mag.* **4**, 392–402 (1902).
32. Gao, H. *et al.* Rayleigh anomaly-surface plasmon polariton resonances in palladium and gold subwavelength hole arrays. *Opt. Express* **17**, 2334–2340 (2009).
33. Cheng, H.-C., Ben-David, I. & Wu, S.-T. Five-Primary-Color LCDs. *J. Display Technol.* **6**, 3–7 (2010).
34. Garini, Y., Young, I. T. & McNamara, G. Spectral imaging: principles and applications. *Cytometry A* **69A**, 735–747 (2006).
35. Logeeswaran, V. J. *et al.* Ultrasmooth Silver Thin Films Deposited with a Germanium Nucleation Layer. *Nano Lett.* **9**, 178–182 (2009).
36. Nagpal, P., Lindquist, N. C., Oh, S.-H. & Norris, D. J. Ultrasmooth Patterned Metals for Plasmonics and Metamaterials. *Science* **325**, 594–597 (2009).
37. Johnson, T. W. *et al.* Highly reproducible near-field optical imaging with sub-20-nm resolution based on template-stripped gold pyramids. *ACS Nano* **6**, 9168–9174 (2012).
38. Park, J. H. *et al.* Single-crystalline silver films for plasmonics. *Adv. Mater.* **24**, 3988–3992 (2012).

Acknowledgements

We acknowledge the financial support from NSF (ECCS 0901324 and CBET-1014957).

Author contributions

B.Z. conceived the idea, and is responsible for the theoretical design, simulation, and experimental demonstration. B.Z. and Y.G. proposed the transparent display concept and conducted numerical simulations. B.Z. and F.J.B. clarified the underlying physics for ELT phenomenon. F.J.B. directed the project. All authors discussed the results and contributed to the manuscript.

Additional information

Supplementary information accompanies this paper at http://www.nature.com/scientificreports

Competing financial interests: The authors declare no competing financial interests.

How to cite this article: Zeng, B., Gao, Y. & Bartoli, F.J. Ultrathin Nanostructured Metals for Highly Transmissive Plasmonic Subtractive Color Filters. *Sci. Rep.* **3**, 2840; DOI:10.1038/srep02840 (2013).